Eur. Phys. J. A **1**, 285–297 (1998)

THE EUROPEAN PHYSICAL JOURNAL A

Shape coexistence near the double-midshell nucleus ^{111}Rh

G. Lhersonneau[1], B. Pfeiffer[2], J. Alstad[3], P. Dendooven[1], K. Eberhardt[2], S. Hankonen[1], I. Klöckl[2], K.-L. Kratz[2], A. Nähler[2], R. Malmbeck[4], J.P. Omtvedt[3], H. Penttilä[1], S. Schoedder[2], G. Skarnemark[4], N. Trautmann[2], J. Äystö[1]

[1] Department of Physics, University of Jyväskylä, P.O.Box. 35, FIN-40351, Jyväskylä, Finland
[2] Institut für Kernchemie, Universität Mainz, Fritz-Strassmann-Weg 2, D-55128 Mainz, Germany
[3] Department of Chemistry, University of Oslo, N-0315 Oslo, Norway
[4] Department of Nuclear Chemistry, Chalmers University of Technology, S-41296 Göteborg, Sweden

Received: 25 June 1997 / Revised version: 10 September 1997
Communicated by P. Armbruster

Abstract. The decay of ^{111}Ru obtained from fast on-line chemical and mass separation has been investigated by β-γ-t and γ-γ coincidence techniques. Earlier spin and parity assignments of ^{111}Rh levels based on extrapolations of level systematics are confirmed. In particular, the K=1/2 intruder band is supported by the hindrance of E2 transitions between deformed and spherical states and enhancement of intraband E2 transitions. The excitation energies of intruder band members in Rh isotopes show a minimum at ^{109}Rh$_{64}$, with two neutrons less than ^{111}Rh at the N=66 midshell. This trend, which differs from the one in the higher-Z neighbouring elements Ag and Cd with minima at N=66, follows the evolution of deformation observed in the lower-Z elements Ru and Mo.

PACS. 27.60.+j $90 \leq A \leq 149$ – 21.10.Tg Lifetimes – 23.20.Lv Gamma transitions and level energies

1 Introduction

The odd mass Rh and Ag isotopes have been extensively studied [1–5], motivated by the presence of low-lying states of seniority v=3 and the identification of a K=1/2 intruder band at rather low excitation energy. This band originates from the strongly down-sloping character of the [431]1/2 proton orbital, which, at large deformation, overcomes the Z=50 major shell gap and intrudes among the spherical configurations built on the $g_{9/2}$ and $p_{1/2}$ subshells. In $_{45}$Rh isotopes, half of the $g_{9/2}$ proton subshell is filled. With N=66, ^{111}Rh is situated at the neutron midshell, halfway between the N=50 and N=82 major shell closures. Hence, collective features should be well developed.

Systematical decay studies of neutron-rich Ru to Rh isotopes were performed by Kaffrell et al. [2,5] at the TRIGA reactor in Mainz. They used the fast chemical separation method SISAK [6,7] to isolate Ru from the fission product mixture. In the last paper of this group, Rogowski et al. [8] presented a level systematics including ^{111}Rh, but did not report on transitions in its level scheme. Other studies using proton-induced fission were performed at the IGISOL mass separator in Jyväskylä. Decay schemes of ^{111}Ru and ^{113}Ru to their Rh daughters were presented in [9] and are included in the recent compilation of the Table of Isotopes [10]. The goal of this work was to establish a more detailed decay scheme of ^{111}Ru to ^{111}Rh, allowing to test the extrapolations of levels presented in [8]. For this purpose, particular attention has been devoted to level lifetime measurements as a key for the identification of the nature of these levels. It is well known, from previous studies of the lighter Rh isotopes [5], that transitions between deformed and spherical levels are strongly retarded whereas large collectivity develops within the members of the intruder band. The experiment also provides an estimate of the perspectives for further experiments on very neutron-rich Rh isotopes, allowing systematic studies of the spherical and deformed intruder states beyond the neutron midshell.

Correspondence to: G. Lhersonneau

2 Experiments

2.1 Fast chemical separation

Neutron-rich ruthenium isotopes were produced by thermal neutron-induced fission of ^{249}Cf (350 μg target) at the TRIGA-reactor in Mainz and chemically separated from other fission products using the SISAK technique [6]. By means of a gas-jet system, the fission products, attached to aerosol particles, were continuously transported from the target site near the reactor core to a degassing unit. Carried by nitrogen at a flow rate of 2 l/min, they entered the SISAK-degasser within approximately 1 s. There, they were dissolved and the transport gas together with the noble fission gases were removed. The activity was dissolved in 0.4 M H_2SO_4 containing 0.015 M $Ce(SO_4)_2$ and 10^{-4} M

$RuCl_3$-carrier. $Ce(SO_4)_2$ was added to oxidize ruthenium to RuO_4. The aqueous phase was kept at a temperature of about 60° C to obtain a fast oxidation. In a subsequent step with a mini-centrifuge (30,000 rpm, 0.3 ml volume), the aqueous phase was contacted with carbontetrachloride to extract almost quantitatively ruthenium tetroxide [7] into the organic phase within 0.1 s. No additional decontamination of the organic phase was necessary. After separation, the organic phase was pumped with a flow rate of 1.5-2 ml/s through a cylindrical teflon cell with a volume of 2 ml. It took about 3.5 s until the activity reached the cell placed in the center of the detector set-up.

The detector setup, used previously for similar measurements [11], consisted of a thin plastic scintillator for β-particle and two Ge-detectors for γ-ray measurements. The β-particles passing through the plastic scintillator provided a trigger signal for the acquisition and a fast timing signal. One of the Ge detectors was of planar type with 0.6 keV FWHM energy resolution at 122 keV and an excellent timing response. The FWHM for prompt β-γ events was 7 and 4 ns for γ-ray energies of 100 keV and 400 keV, respectively. The other detector, a large-volume coaxial Ge with a relative efficiency of 55% and 1.9 keV energy resolution at 1.33 MeV, was used in coincidence with the planar detector in order to investigate the level schemes of the studied nuclei and to identify possible contaminations.

The lifetime measurements of Rh levels were performed using the delayed-coincidence technique between β-particles and γ-rays following the decay of chemically isolated Ru parent nuclides. It is important to remember that, using the centroid-shift method with β-γ coincidences, the observed centroid-shifts seldom correspond to the meanlives (τ) of the levels depopulated by the selected γ-rays. They, instead, are the sums of the meanlives of the levels along the de-excitation path and, in case there are several paths leading to the level of interest, the observed meanlife is a sum, weighted by the intensities of the populations of the various paths. Therefore, the absence of contaminations in the γ-ray gates and a detailed knowledge of the decay scheme are necessary for a reliable interpretation of the observed centroid-shifts. Coincidence events were recorded as energy-energy-time parameter triplets for each detector pair using the GOOSY multiparameter system [12] and sorted off-line.

The experiment lasted about 60 hours. The Ru chemistry was very selective since only traces of ^{136}I, ^{107}Tc and ^{108}Tc were found in the separated fraction. Ruthenium activities from ^{107}Ru to ^{113}Ru could be observed. The main contributions to the spectra were due to ^{109}Ru, ^{110}Ru and ^{111}Ru. Owing to the steady transport of the active solution, the longer-lived Rh daughter activities were strongly suppressed and did not interfere severely with the measurements. However, an exception was the population of a line at 302.8 keV in ^{107}Rh decay, the intensity of which was about one half of that of the 303.6 keV transition in the decay of ^{111}Ru to ^{111}Rh. In addition, the complex decay scheme of ^{109}Ru turned out to include intense transitions masking some transitions in the decay of ^{111}Ru. Since all these isotopic interferences could not be accurately disentangled, the singles and coincidence data from the chemical separation with SISAK were compared with data from an experiment performed subsequently at Jyväskylä using on-line mass-separation of fission products.

2.2 On-line mass-separation

The experiment at IGISOL was primarily dedicated to the measurement of β-decay Q-values of nuclides in the mass range A = 110 to 115 [13]. The experimental technique of the ion-guide and the performance of the upgraded IGISOL facility have been reported recently [14,15]. The detector setup, with a β-detector and two Ge-detectors for the γ-ray measurements, was similar to the one described above and in recent publications [16,17]. The main difference was that a plastic-scintillator telescope was used for the detection of β-particles. It consisted of a thin transmission detector in front of the thick plastic scintillator delivering the full-energy signal for the determination of β-end-point energies. The planar Ge-detector had an area of 10 cm^2 and a thickness of 1 cm. The coaxial Ge-detector of 37% relative efficiency was used to record γ-rays with energies up to 4.8 MeV. This measurement was not devoted to lifetime measurements. Hence, the timing resolution achieved with both plastic-Ge detector pairs was about one order of magnitude poorer than in the SISAK experiment. The data acquisition was performed with the multiparameter system VENLA designed at the Accelerator Laboratory in Jyväskylä [18]. The level scheme of ^{111}Rh was constructed from β-γ and γ-γ coincidence matrices created off-line. The acquisition of coincidence events in the A=111 mass chain lasted for only about 20 hours. Nevertheless, the counting statistics was higher than in the SISAK experiment by about a factor of 7.

2.3 Analysis

The experiments enabled the improvement of the decay scheme of ^{111}Ru to ^{111}Rh. For the strongest lines, comparison of the relative γ-ray intensities in the β-gated γ-ray energy spectra obtained after chemical and mass separation was sufficient to assign the transitions to the ^{111}Ru decay or identify them as contaminations. Coincidence relationships were used to assign the weaker transitions to the ^{111}Rh level scheme. Their intensities were deduced from the number of coincidence counts in suitable gates. Energy and detector-efficiency calibrations for the SISAK measurement were mainly made internally by using the detailed decay scheme of ^{109}Ru [5], while an ^{152}Eu standard source and A=97 data for the high energy range [10] were used for the measurement at IGISOL. As long as the transitions belonged exclusively to the decay of ^{111}Ru, no significant deviations between the energies and intensities deduced from these two different experiments were observed.

Level lifetimes were deduced from the SISAK data only, because of the much better timing resolution. The

IGISOL data were nevertheless used to check for possible occurrence of discrepancies arising from yet unidentified contaminations. A few level lifetimes were long enough to be analysed by the slope method. For the shorter ones, the centroid-shift method was used. The correction of the time spectrum due to the background under the γ-ray peaks is especially critical in this case. The algorithm of [19] corrects to first order for the number of counts in the time spectrum due to the Compton-background. The variation of the centroid of the background time spectrum versus energy is less accurately corrected but the error is still negligible in practice. The determination of the prompt curve, which is the location of the centroids of the prompt transitions for the various γ-ray energies, is difficult due to the scarcity of accurate references in this nuclear region. For the higher-energy part of the curve, collective transitions between high-lying levels in even-even Pd nuclei are fast enough to be regarded as prompt within the accuracy of this measurement. Moreover, the halflives for the transitions from the first excited 2^+ states are accurately known [10,20]. For energies above 200 keV the systematical error on the position of the prompt curve is estimated to be less than 0.15 ns. For γ-ray energies below 200 keV, the prompt curve bends and becomes more difficult to determine. We have used the fact that the centroids for the lines at 165 and 151 keV which depopulate the same level in ^{108}Rh [10] must have the same shift with respect to the prompt curve. Furthermore, it is reasonable to assume the corresponding 1^+ levels in ^{108}Rh and in ^{110}Rh [21] to be prompt. The lifetimes for the ^{111}Rh transitions of interest in this low-energy region are anyway long enough to be analysed by the slope method.

3 Results

3.1 Decay scheme of ^{111}Ru to ^{111}Rh

The decay scheme, see Fig. 1, is constructed using the γ-γ coincidence data. In addition, the new and strong lines of 2034 and 2215 keV, observed in the single spectra of both experiments, and the weaker 567 and 1039 keV γ-rays are placed as ground-state transitions using level energy differences. The list of γ-rays and coincidence relationships is shown in Table 1. Conversion coefficients reported in [9] establish the following multipolarities: 79 keV (M1), 91 keV (M1+E2), 137 keV (M1), 211 keV (M1), 304 keV (E2) and 382 keV (M1,E2). In this work, conversion coefficients for the 79 and 91 keV transitions were obtained from intensity balance considerations in appropriate gates, see Table 1. The levels shown by Rogowski et al. [8] and Penttilä [9] are confirmed. Nevertheless, this work allows a significant extension of the ^{111}Rh level scheme.

3.1.1 New features of the ^{111}Rh level scheme

The existence of a 189 keV doublet was reported in [9]. It is resolved into two transitions of 188.8 and 189.1 keV in cascade, owing to new γ-γ coincidence data. The placement of these transitions is confirmed by the analysis of the delayed coincidences, Sect. 3.2.2. The 189.1 keV transition is the most intense one and is placed as the lowest one in the cascade. Both the 1686 and 1730 keV γ-rays are also doublets and two new transitions are placed which depopulate a new level at 2127 keV. Other corrections concern the intensities of some transitions. The intensity of the 137 keV transition, which is also placed in the level scheme of ^{111}Pd, has been somewhat overestimated in [9].

Furthermore, new transitions between low-energy levels, which clearly are important for determining the spins of the levels, and new high-energy transitions have been found. The weak transition of 45.5 keV between the 441 and 395 keV levels is not observed as a γ-ray. However, its existence is supported by the 91–223 coincidence relationship. This transition is expected by analogy with the scheme of ^{109}Rh, where it plays a role as a member of the intruder band [5]. Another new and strong transition is placed from the 2034 keV level to the ground state. Although it is the third most intense transition in the ^{111}Ru decay scheme it was not reported earlier. Preliminary analysis of the β-end-point energies from the IGISOL experiment also support this placement [13]. Finally, new levels at 2127 and 2215 keV are introduced.

The intensities of the β-branches are strongly modified by these new transitions. The β-feedings to the low-energy levels now become very small. The ground-state branching decreases from 60% [9] to 50%, since a large part of the β-feeding intensity moves up to the levels at 1054 keV and above. The logft values indicate the same parity for the ground state of the mother nucleus ^{111}Ru, the high-lying levels in ^{111}Rh and its ground state.

The spin assignments are not systematically discussed here. Either the levels were reported by [8] and there is no discrepancy between their assignments and the decay patterns observed in this work, or, for the high-energy levels, only tentative spin and parity assignments can be made. However, the 2127 keV level, which leads to the spin and parity assigment of ^{111}Ru, is discussed below.

3.1.2 Spin and parity of ^{111}Ru

Level systematics indicate $I^\pi=7/2^+$ for the ground state of ^{111}Rh [8,9]. Based on the allowed character of the ground-state β-branch (logft = 5.0), the ground state of ^{111}Ru has even parity and $I\geq 5/2$. The new 2127 keV level, fed via another allowed β-branch with also a logft value of 5.0, must have even parity and $I\geq 3/2$. The depopulation of the 2127 keV level by a large number of transitions to states all with spins smaller or equal to 5/2, including the $1/2^-$ level at 493 keV, indicates $I^\pi=3/2^+$. The next possible choice, $5/2^+$, would have to face the lack of decays to $7/2^+$ levels as well as the high branching ratio of the M2 transition to the $1/2^-$ state. With allowed β-feeding to the $7/2^+$ ^{111}Rh ground state and to the $3/2^+$ 2127 keV level, the ^{111}Ru ground state has to be $I^\pi=5/2^+$. This is also the spin and parity of its ^{107}Ru and ^{109}Ru neighbours [2,5].

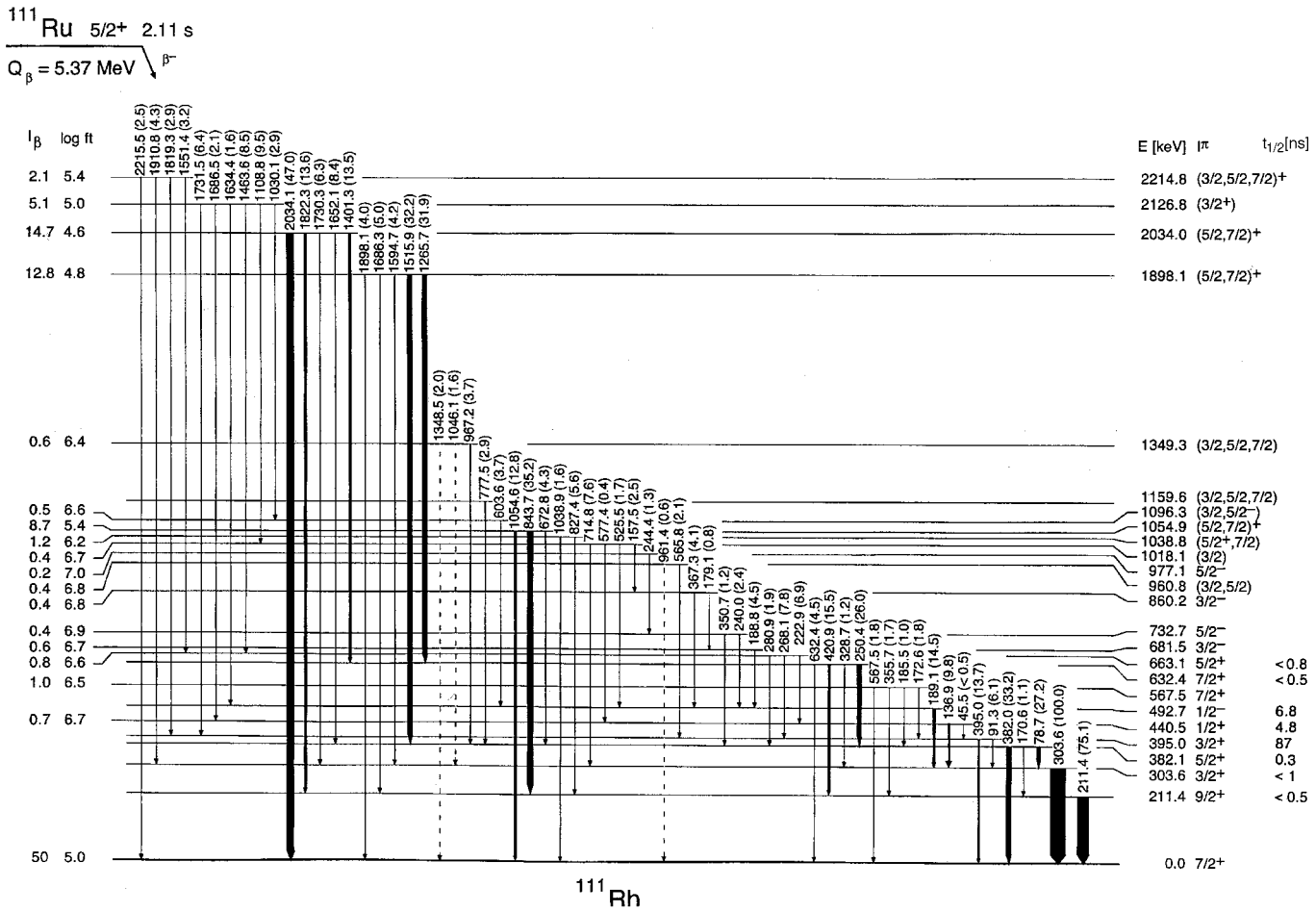

Fig. 1. Decay scheme of ^{111}Ru to ^{111}Rh. Dashed transitions have not been included in the calculation of intensity balances. Spin assignments without brackets are those made from systematics by Rogowski et al. [8]

3.2 Level-lifetime measurements

The results from this work are listed in Table 2. A plot of centroids of the time spectra versus γ-ray energy in the planar Ge-detector is shown in Fig. 2. The interpretation of the experimental shifts is presented in the following section for new results and the cases for which no straightforward relationship to a single level lifetime exists. Selected time spectra, discussed in some detail in the text, are shown in Figure 3.

3.2.1 The 427 keV level in ^{109}Rh

About 70% of the 427 keV peak area is calculated to be due to the transition in ^{109}Rh, while another one belongs to the scheme of ^{109}Pd [10]. The lifetime of 8(1) ns for the 427 keV level in ^{109}Rh [10] cannot be confirmed. Such a halflife should have been visible as a slope in the time spectrum (see Fig. 3). An alternative decay of the 427 keV level is the 68 keV transition, followed by the 359 keV transition. Taking into account the centroid shifts of the 427 and 359 keV transitions, we adopt an upper limit of 0.5 ns for the 427 keV level. It is probable that the 8 ns value quoted in [22] corresponds to the apparent slope due to the finite timing resolution in the experiment of [5] instead of to the actual halflife of the level.

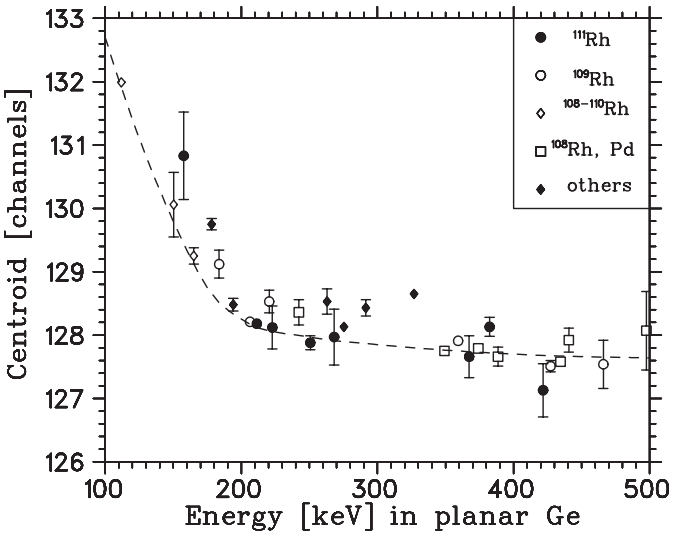

Fig. 2. Centroids of the β-γ-time spectra for the transitions discussed in the text. The prompt curve is shown as a *dashed line*. The conversion is 1.03 ns/channel

Table 1. γ-rays assigned to the decay of ^{111}Ru to ^{111}Rh. For absolute γ-ray intensities per decay, multiply the relative intensities with 0.165×10^{-2}. Transitions reported for the first time are marked with ^{n}. A ^{u} indicates that the transition cannot be assigned unambiguously to ^{111}Rh. It is either seen in the singles spectra only and could fit as a ground-state transition or there is a weak coincidence relationship but without further support. In this case, the quoted intensity is calculated assuming the tentative placement shown between brackets.

Energy [keV]		Intensity [%]		Placed from	to	Coincidences and remarks
45.5	^{n}	< 0.5		441	395	$I_{\gamma+e^-}$ = 2.1(8), M1+E2
78.7	(2)	27.2	(44)	382	304	(186), 250, 304, α=0.62(30), M1
91.3	(3)	6.1	(9)	395	304	(172), (223), 268, 304, α=0.86(47), M1+E2
136.9	(3)	9.8	(15)	441	304	223, 304
157.5	(3)^{n}	2.5	(4)	1019	861	(179), 189, 304, 368
170.6	(2)^{n}	1.1	(3)	382	211	(211), (250)
172.6	(5)^{n}	1.8	(6)	568	395	(91), (304), (395)
179.1	(4)^{n}	0.8	(2)	861	682	(158), 189, (304)
185.5	(2)^{n}	1.0	(2)	568	382	(78)
188.8	(5)	4.5	(10)	682	493	189, 304
189.1	(2)	14.5	(21)	493	304	158, 179, 189, 240, 304, (604)
191.3	(2)^{u}	3.6	(4)	(586	395)	can be in ^{111}Pd
205.8	(4)^{u}	0.5	(2)	(417	211)	(211)
211.4	(2)	75.1	(61)	211	0	(250), (280), (356), (368), 397, 421
222.9	(4)	6.9	(7)	663	441	(91), 137, 304, (395)
240.0	(3)^{n}	2.4	(4)	733	493	189, 304
244.4	(5)^{n}	1.3	(3)	977	733	189, (240), 304
250.4	(2)	26.0	(16)	632	382	78, 304, 382
268.1	(3)^{n}	7.8	(11)	663	395	91, 304, 395
279.9	(4)^{u}	1.6	(3)	(491	211)	211
280.9	(4)^{n}	1.9	(4)	663	382	78, 304, 382
295.4	(3)^{n}	0.7	(2)	977	682	(189)
303.6	(2)	100.		304	0	78, 91, 137, (172), (179), (186), 189, 223, 240, 250, 268, (381), (604)
328.7	(4)^{n}	1.2	(3)	632	304	(304)
350.7	(4)^{n}	1.2	(3)	733	382	78, (382)
355.7	(4)^{n}	1.7	(4)	568	211	211
367.3	(3)^{n}	4.1	(8)	861	493	158, 189, 304
381.4	(5)^{u}	1.2	(4)	(685	304)	(304)
382.0	(2)	33.2	(30)	382	0	(186), 250, (280)
395.0	(3)	13.7	(28)	395	0	172, (223), 268
397.0	(4)^{n}	2.4	(4)	(608	211)	211
420.9	(2)	15.5	(14)	632	211	211
449.7	(4)^{n}	1.1	(3)	(661	211)	(211)
483.9	(5)^{n}	0.7	(2)	977	493	(189)
519.5	(5)^{n}	0.4	(2)	961	441	(137)
525.5	(4)^{n}	1.7	(6)	1019	493	(189), (304)
550.0	(5)^{u}					(78), (91)
554.0	(5)^{u}	1.1	(3)	(936	382)	(78)
565.8	(5)^{n}	2.1	(6)	961	395	(91), (395)
567.5	(4)^{n}	1.8	(3)	568	0	
577.4	(5)^{n}	0.4	(2)	1019	441	(137)
603.6	(3)^{n}	3.7	(6)	1098	493	189, 304
632.4	(3)	4.5	(9)	632	0	
672.8	(4)^{n}	4.3	(8)	1054	382	78, (304)
714.8	(3)^{n}	7.6	(14)	1019	304	304
717.6	(5)^{n}	1.7	(4)	1349	632	(250)
777.5	(4)^{n}	2.9	(9)	1160	382	78, (304)
827.4	(3)^{n}	5.6	(8)	1039	211	211
843.7	(2)	35.2	(38)	1054	211	211
961.4	(11)^{u}	0.6	(3)	(961	0)	
967.2	(4)^{n}	3.7	(7)	1349	382	78, (304), (382)
1030.1	(3)^{n}	2.9	(6)	2127	1098	189, 304, (604)
1038.9	(4)^{n}	1.6	(3)	1039	0	
1046.1	(12)^{u}	1.6	(8)	1349	304	(304)

Table 1. Continued

Energy [keV]		Intensity [%]		Placed from	to	Coincidences and remarks
1054.6	(3)	12.8	(17)	1054	0	
1108.8	$(3)^n$	9.5	(13)	2127	1019	158, 189, 304, (368)
1265.7	(2)	31.9	(37)	1898	632	78, 211, 250, 304, 382, 421
1348.5	$(2)^u$	2.0	(4)	(1349	0)	
1398.2	$(7)^u$	1.8	(6)	(1781	382)	(78)
1401.3	(4)	13.5	(18)	2034	632	78, 211, 250, 304, 382, 421
1445.6	$(5)^n$	0.9	(4)	2127	682	(189)
1463.6	$(3)^n$	8.5	(12)	2127	663	(78), (91), 137, 223, 268, (304)
1515.9	(3)	32.2	(38)	1898	382	78, 304, 382
1551.4	$(4)^n$	3.2	(7)	2215	663	(137), (223)
1594.7	$(5)^n$	4.2	(9)	1898	304	(304)
1634.4	$(7)^n$	1.6	(7)	2127	493	(189)
1652.1	$(4)^n$	8.4	(12)	2034	382	78, (304), (382)
1686.3	(5)	5.0	(9)	1898	211	211
1686.5	$(5)^n$	2.1	(6)	2127	441	137
1730.3	(4)	6.3	(10)	2034	304	304
1731.5	$(5)^n$	6.4	(15)	2127	395	(91)
1819.3	$(6)^n$	2.9	(9)	2215	395	(91)
1822.3	(4)	13.6	(19)	2034	211	211
1898.1	(4)	4.0	(9)	1898	0	
1910.8	$(5)^n$	4.3	(9)	2215	304	304
2034.1	$(3)^n$	47.0	(58)	2034	0	
2215.5	$(4)^n$	2.5	(6)	2215	0	

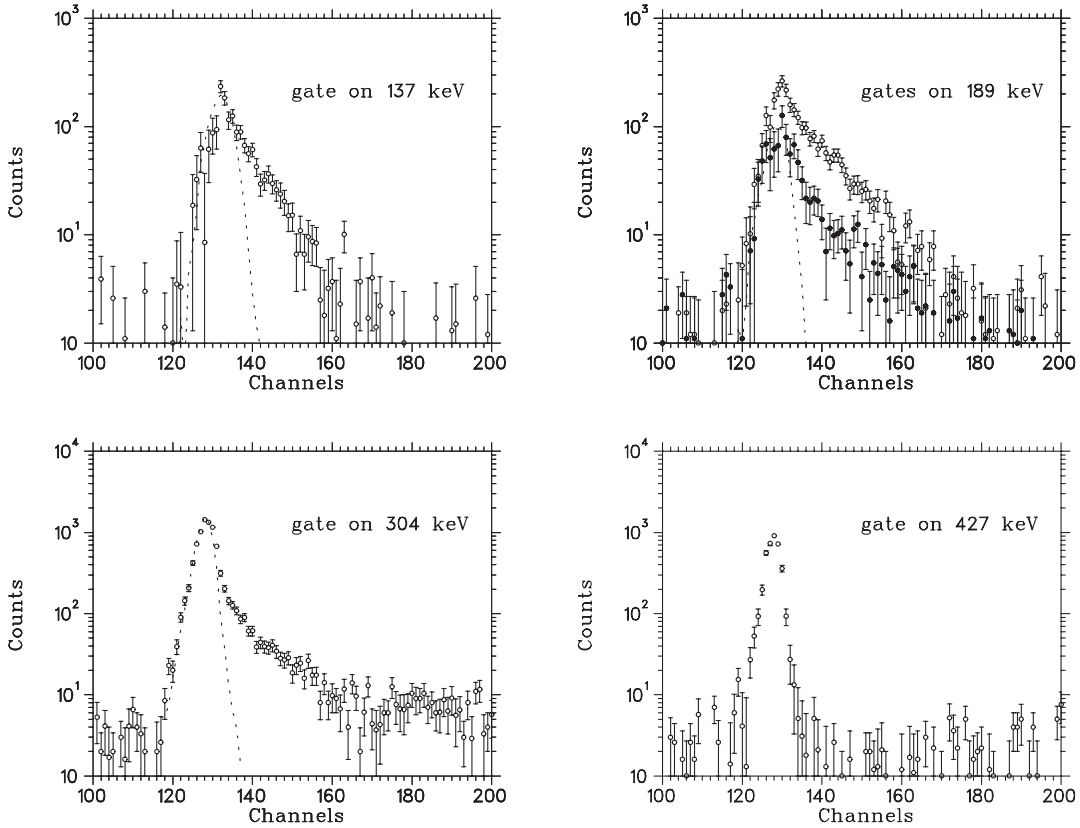

Fig. 3. Beta-gamma-time spectra for γ-rays of 137 keV (^{111}Rh+^{111}Pd), 189 keV (^{111}Rh doublet, *full* (resp. *open*) *circles* are used for the gates on the left- (resp. right)-hand sides of the peak), 304 keV (^{111}Rh+^{107}Pd) and 427 keV (^{109}Rh). The *dotted lines* represent the response function at the energies of interest. These spectra are discussed in the text

Table 2. Halflives measured in this work. Experimental values are from centroid-shifts unless marked by [a], in which case the slope method was used. If the centroid shift is zero within 1 standard deviation (σ), an upper limit of 3 σ is adopted. An average on several transitions is indicated by [b]. The estimate using the top of the time distribution of the 304 keV transition is marked with [c])

Isotope	Level [keV]	γ-ray [keV]	$t_{1/2}$ [ns] Experimental		Ref.
^{109}Rh	206	206	0.02(14)	< 0.5	
	359	359	0.12(12)	< 0.5	
	374	116	34(2)[a]		33(2) [5]
	410	184	0.43(23)		
	427	427	-0.13(18)	<0.5	8(1) [22]
	478	221	0.32(19)	< 0.6[b]	
		252	-0.01(32)		
^{111}Rh	211	211	0.03(15)	< 0.5	
	304	304		<1[c]	
	382	382	0.29(15)		
	395	395	64(10)[a]		87(8) [5]
	440	137	4.8(5)[a]		
	493	189	6.8(4)[a]		
	632	421	-0.54(32)	< 0.5[b]	
		250	-0.06(16)		
	663	268	0.04(34)	< 0.8[b]	
		223	0.04(28)		
^{109}Pd	327	327	0.61(11)	0.57(15)[b]	
		178	0.79(19)		
		291	0.40(15)		
^{111}Pd	276	276	0.16(12)		

It is difficult to estimate the lifetime of the 478 keV level. The 221 keV transition actually is a doublet in ^{109}Rh [5]. The 252 keV transition gives an additional value. An upper limit of 0.6 ns is finally adopted.

3.2.2 Levels in ^{111}Rh

For the 211 keV $9/2^+ \rightarrow 7/2^+$ ground-state transition, the observed shift corresponds to $t_{1/2}$ <0.5 ns. A minor contribution of about 2% in the peak is due to a line in the level scheme of ^{109}Pd [22] and an even weaker one from a line in ^{113}Rh [9,10]. This transition is the one between the seniority v=1 and v=3 levels discussed in Sect. 4.1.1.

The $3/2^+$ level at 304 keV decays to the $7/2^+$ ground-state by an E2 transition. The time spectrum for the 304 keV gate, Fig. 3, is very complex. Firstly, as mentioned previously, about one third of the peak intensity is due to a line in ^{107}Pd. This line could correspond to the 327 keV line in ^{109}Pd for which a 0.6 ns halflife is measured (see section 3.2.4). Secondly, the ground-state transition in ^{111}Rh, which accounts for the remaining two thirds of the peak area, is the lower member of various cascades, some of which involve delayed transitions discussed in the following. A meaningful analysis of this complex time spectrum is not possible. Nevertheless, the presence of a fairly short component, the intensity of which is larger than the contribution of the line in ^{107}Pd, suggests that the 304 keV level itself is not very much delayed. We tentatively adopt an upper limit of 1 ns.

According to [8] the halflife of 87(8) ns for the 395 keV level ($I^\pi=3/2^+$) is the first piece of evidence for the existence of a deformed level in ^{111}Rh. In our experiment a value of 64(10) ns is obtained, which is in reasonable agreement with the result of [8]. However, we regard our value as less reliable, due to the short range of about 300 ns available for fitting peak and background and our lower statistics. This lifetime is responsible for the tail observed in the time spectrum of the 304 keV transition, Fig. 3, since the 395 keV level populates the 304 keV level via the 91 keV transition.

The 440 keV $I^\pi=1/2^+$ level was assigned as the head of the K=1/2 intruder band [8]. It decays to the 304 keV level by the 137 keV transition. The analysis of the time spectrum of this transition, see Fig. 3, by the slope method yields $t_{1/2}$=4.8(5) ns, which is a new lifetime value. The prompt component visible near the top of the spectrum is due to another transition of 137 keV placed in ^{111}Pd, as already mentioned in Sect. 3.1.1.

Another long lifetime is observed for one of the transitions in the doublet at 189 keV. Figure 3 shows the time spectra for gates on the left and right-hand sides of the 189 keV peak. The fraction of the prompt component is the lowest in the spectrum for the highest-energy gate, indicating that the 189.1 keV transition is the lowest-lying one in the scheme and that it depopulates the level at 493 keV. This is in agreement with the γ-γ coincidence data. The analysis of the slope yields a new value of $t_{1/2}$=6.8(4) ns for the $I^\pi=1/2^-$ level at 493 keV.

It is interesting to note that, already in the more than 20-years old delayed-coincidence measurements of fission products from a ^{252}Cf source, Clark et al. [23] reported a 303.7 keV γ-ray belonging to mass 111(1) associated with halflives of 4.1(8) and 67(22) ns and another γ-ray of 189.2 keV, belonging to the mass 112(1), with a halflife of 5.7(11) ns. Their transition energies and halflife values compare very well with our results. However, they also assigned a 60.3 keV transition to ^{111}Rh with a halflife of 45(6) ns which is not observed in our work.

The $I^\pi=5/2^+$ level at 663 keV has its main decays to the 395 and 440 keV levels. The average of the lifetime values, deduced from the centroid shifts for the 223 keV and 268 keV transitions, corresponds to $t_{1/2}$=0.04(24) ns. The upper limit of 0.8 ns at 3 standard deviations is adopted. This level was proposed as another member of the intruder band [8].

3.2.3 The 263 keV level in ^{113}Rh

Despite its short β-decay halflife of 0.8 s, ^{113}Ru [24] was separated in the SISAK experiment. The strongest coincidences in this decay, belonging to the cascade of the 338 and 263 keV transitions in ^{113}Rh [9,10], are observed. The value of $t_{1/2}$=0.49(19) ns for the 263 keV level (assumed to correspond to the 304 keV level in ^{111}Rh, see Fig. 4) is preliminary, since the interference of possible additional delayed feedings cannot be evaluated.

Table 3. Summary of properties of ^{111}Rh levels populated in β-decay of ^{111}Ru. Logft values are calculated with $T_{1/2}$ = 2.11 s and Q_β = 5.37 MeV [25]. Their limits are given at 2 standard deviations. Spin and parity assignments are based on systematics of level energies [8] and transition rates from this work. New spin and parity assignments are given within brackets

Energy [keV]		β-feeding [%]		log(ft)	I^π	Halflife [ns]	Configuration	Level reported by
0.0		50.0	10.0	5.0	$7/2^+$			
211.4	(2)	0.1	(13)	> 6.3	$9/2^+$	< 0.5	$g_{9/2}$	[8,9]
303.6	(2)	-0.3	(20)	> 6.0	$3/2^+$	< 1		[8,9]
382.1	(2)	-0.6	(20)	> 6.0	$5/2^+$	0.3(2)		[8,9]
395.0	(2)	0.3	(8)	> 6.3	$3/2^+$	87(8)	[431]1/2	[8,9]
440.5	(3)	0.7	(4)	6.7	$1/2^+$	4.8(5)	[431]1/2	[8,9]
492.7	(3)	-0.6	(5)	> 6.9	$1/2^-$	6.8(4)	$p_{1/2}$	[8,9]
567.5	(2)	1.0	(3)	6.5	$7/2^+$		[431]1/2	[8]
632.4	(2)	0.3	(8)	> 6.2	$7/2^+$	< 0.5		[8,9]
663.1	(3)	0.8	(4)	6.6	$5/2^+$	< 0.8	[431]1/2	[8,9]
681.5	(6)	0.6	(2)	6.7	$3/2^-$			[8,9]
732.7	(3)	0.4	(2)	6.9	$5/2^-$			[8]
860.2	(4)	0.4	(2)	6.8	$3/2^-$		$p_{3/2}$	[8]
960.8	(6)	0.4	(2)	6.8	(3/2,5/2)			
977.1	(6)	0.2	(1)	7.0	$5/2^-$		$f_{5/2}$	[8]
1018.1	(3)	0.4	(4)	> 6.3	(3/2)			
1038.8	(3)	1.2	(3)	6.2	$(5/2^+,7/2)$			
1054.9	(2)	8.7	(19)	5.4	$(5/2,7/2)^+$			[8,9]
1096.3	(4)	0.1	(2)	> 6.6	$(3/2,5/2^-)$			
1159.6	(4)	0.5	(2)	6.6	(3/2,5/2,7/2)			
1349.3	(4)	0.6	(2)	6.4	(3/2,5/2,7/2)			
1898.1	(2)	12.8	(28)	4.8	$(5/2,7/2)^+$			[9]
2034.0	(2)	14.7	(32)	4.6	$(5/2,7/2)^+$			[9]
2126.8	(2)	5.1	(12)	5.0	$(3/2)^+$			
2214.8	(3)	2.1	(5)	5.4	$(3/2,5/2,7/2)^+$			

3.2.4 The 327 keV level in ^{109}Pd

Several transitions belonging to the level scheme of ^{109}Pd display sizeable centroid shifts, Fig. 2 and Table 2. Shifts are observed for the 327 keV ground-state transition and for the 178 and 291 keV transitions from the 291 keV level, which is populated from the 327 keV level via the 35 keV transition. These shifts can be interpreted as due to the lifetime of the 327 keV level. The small experimental centroid shifts for the transitions of 245 and 276 keV, weakly populated in the decay of the 327 keV level, result from contaminations by very intense transitions placed in the level schemes of ^{109}Rh and ^{111}Pd, respectively. With the assumption of a negligible direct β-feeding to the 291 keV level [10], a halflife of 0.57(15) ns is deduced for the 327 keV level.

4 Discussion

The levels in the heaviest odd-mass Rh isotopes up to ^{109}Rh have been discussed by Kaffrell et al. [2,5]. Rogowski et al. [8] assigned the levels in ^{111}Rh based on the smooth trend of excitation energies versus neutron number, starting from lighter masses for which transfer data were available. Our lifetime measurements put their assignments on a firmer ground. Properties of the levels in ^{111}Rh are listed in Table 3. A summary of transition rates for E2 transitions in the ^{107}Rh, ^{109}Rh and ^{111}Rh isotopes is presented in Table 4. Levels in these isotopes are discussed in the following section. Guided by the fairly smooth evolution of levels versus neutron number, we propose assignments to levels in ^{113}Rh [9,10]. These are included in Fig. 4.

4.1 Even-parity spherical levels

Even-parity levels in odd-mass Rh isotopes are built on the $g_{9/2}$ shell. Spherical I^π=$5/2^+$ and $7/2^+$ levels, observed near 0.5 MeV, originate from the $2^+\otimes g_{9/2}$ coupling. The 444 keV level in ^{113}Rh [9,10] which does not correspond to other low-energy levels in the lighter Rh isotopes could be the $9/2^+$ state of this core + particle configuration. In addition, the large number of particles (or holes) in the $g_{9/2}$ shell is responsible for higher-seniority configurations forming the $7/2^+$ ground state of the neutron-rich Rh isotopes and a low-lying $3/2^+$ level.

4.1.1 The $9/2^+$ single-particle and the $7/2^+$ anomalous-coupling states

The $7/2^+$ and $9/2^+$ states in odd-mass $_{45}$Rh isotopes are close to each other throughout the systematics [10], the

$7/2^+$ level being the lowest one for A≥103. Similar features are also known for the odd-mass $_{47}$Ag isotopes [10]. The $9/2^+$ level is associated with the $g_{9/2}$ single-proton orbital. The low-lying $7/2^+$ state is an example of the well known I=j-1 anomaly [26], based on the j^3 state of seniority 3, where j is the $g_{9/2}$ subshell. In Rh and Ag isotopes, the situation is especially favourable for the occurrence of such states since the $g_{9/2}$ proton shell is the j=l+s intruding orbital before the major Z=50 shell closure which cannot mix with the orbitals of natural (odd) parity. Similar phenomena for N=53 isotones in the Z ≤ 40 region can be regarded as a result of the strong $d_{5/2}$ neutron shell closure [27]. The transitions between the $9/2^+$ and $7/2^+$ states are usually of M1+E2 character, with some retardation of the M1 and enhancement of the E2 components. The presently available K-conversion coefficients of α_k=0.041(7) and 0.037(3) for the 206 keV (^{109}Rh) and 211 keV (^{111}Rh) transitions, respectively [9], do indicate M1 character with a possible admixture of E2. Nevertheless, it is clear that a detailed interpretation requires more accurate measurements of level halflives and of δ(E2/M1) mixing ratios for the $9/2^+$ to $7/2^+$ transitions.

4.1.2 Enhanced E2 transitions from $3/2^+$ and $5/2^+$ states

Rogowski et al. [8] presented a doublet of $3/2^+$ and $5/2^+$ states, the excitation energy of which decreases steadily with increasing neutron number.

The 304 keV level in ^{111}Rh is a $3/2^+$ state. The presence of a fairly prompt component ($t_{1/2}$ < 1 ns) in the time spectrum of the 304 keV E2 transition suggests acceleration with respect to the 6.8 ns single-particle estimate. The halflife of the corresponding 406 keV level in ^{107}Rh is not known but, for the 359 keV level in ^{109}Rh the upper limit of 0.5 ns from this work corresponds to an enhancement of more than 6. These low-lying $3/2^+$ states are not present in the level schemes of the respective $_{47}$Ag isotones, a fact which suggests a high seniority [2,26].

The level at 382 keV in ^{111}Rh was assigned $I^\pi=5/2^+$ by Rogowski et al. [8] and $t_{1/2}$=0.29(15) ns is deduced from this work. The newly placed 170 keV transition to the $9/2^+$ level is consequently an E2 transition with 6(3) times the single-particle rate. For the $3/2^+$ level at 427 keV in ^{109}Rh, the upper limit of 0.5 ns from this work implies a rate larger than 2.8 single-particle units for the corresponding 221 keV E2 transition to the $9/2^+$ state at 206 keV.

Thus, the experimental decay rates for E2 transitions from these $3/2^+$ and $5/2^+$ levels in ^{109}Rh and ^{111}Rh are consistent with moderate enhancements.

4.1.3 A tentative excited $7/2^+$ state in ^{111}Rh

Rogowski et al. [8] also presented a level systematics for a higher-lying $7/2^+$ state, proposed to be the 632 keV level in ^{111}Rh. However, $I^\pi=5/2^+$ is reported in [9,10]. The 632 keV level decays to the $9/2^+$ level at 211 keV via the 421 keV transition and to the $3/2^+$ level at 304 keV via the newly placed 329 keV transition. Depending on the spin of the 632 keV level, one or the other of these transitions must be an E2. Unfortunately, the 0.5 ns upper limit for the halflife of the 632 keV level does not clearly favour one or the other assignment. We tentatively adopt $7/2^+$ [8] because of level systematics.

4.2 Odd-parity spherical levels

Odd-parity levels are built on the $p_{1/2}$ shell. The systematics [8] shows that the excitation energies of odd-parity levels increase rapidly with increasing neutron number, reflecting the increasing separation of the $g_{9/2}$ and $p_{1/2}$ proton orbitals, the $g_{9/2}$ level becoming more bound by the addition of neutrons. Nevertheless, the excitation energies relative to the $p_{1/2}$ single-particle level decrease with increasing neutron number. This behaviour, also exhibited by the even-parity states, follows the trends of the 2^+ phonon-energies in the neighbouring Ru and Pd isotones [10].

4.2.1 The $1/2^-$ single-particle state

The halflife of the 493 keV level in ^{111}Rh has been determined in this work to be 6.8(4) ns. This yields a rate of 6.5×10^{-6} single-particle units (s.p.u.) for the E1 transition to the $3/2^+$ level at 304 keV. In ^{107}Rh, the only decay mode of the $1/2^-$ level is an E3 transition to the $7/2^+$ ground state. In ^{109}Rh, E1 transitions to lower-lying $1/2^+$ and $3/2^+$ states compete favourably with the E3 decay. The 33 ns halflife of the $1/2^-$ level at 374 keV was first measured by Kaffrell et al. [5] and could be confirmed in this work. Rates of 4.8×10^{-8} and 5.8×10^{-6} s.p.u. are deduced for the 148 and 116 keV E1 transitions to the lower-lying $3/2^+$ and $1/2^+$ levels, respectively. These rates fit well into the systematics of E1 transition rates. However, the $1/2^+$ and $3/2^+$ levels in ^{109}Rh belong to the intruder band as discussed later. The spherical $3/2^+$ level in ^{109}Rh is only 15 keV below the $1/2^-$ level and the transition could not be observed.

4.2.2 Higher-lying odd-parity levels

Pairs of $(3/2, 5/2)^-$ levels were shown by Rogowski et al. [8]. Kaffrell et al. [2,5] have performed transfer reactions for $^{107-109}$Rh, which indicate a $2^+\otimes p_{1/2}$ configuration for the lowest doublet and the $p_{3/2}$ and $f_{5/2}$ single-particle states for the highest one. For ^{111}Rh, the doublets of $(3/2, 5/2)^-$ levels are proposed at (682, 733) and (860, 977) keV, respectively [8]. In this work it was not possible to obtain meaningful lifetime information for these weakly populated levels. Nevertheless, it could be verified that their depopulation is consistent with the proposed assignments.

4.3 The K=1/2 intruder band

The existence of K=1/2 intruder bands in Rh and Ag isotopes is well known [3,4]. The [431]1/2 proton orbital, the origin of which is the spherical $d_{5/2}$ subshell above the Z=50 shell gap, comes down very fast with increasing prolate deformation and appears at moderate excitation energies near the N=66 neutron midshell [1]. In ^{107}Rh, ^{109}Rh and ^{111}Rh, due to the large negative decoupling parameters, the $3/2^+$ level lies below the $1/2^+$ band head. In [2,5] hindrances have been reported for the E2 decays from the $3/2^+$ levels at the bottom of the bands to the $7/2^+$ spherical ground states. Rogowski et al. [8] already noticed that the excitation energies of the deformed bands show a minimum, exactly at the N=66 neutron midshell for Ag isotopes, but shifted to N=64 for Rh isotopes. Examination of the 2^+ energies [10] and of deformations deduced from lifetime measurements of 2^+ states in the even-even neighbours [11,20] shows that the collectivity is also the strongest at N=64 for the lower-Z elements Ru and Mo. The energies of the 2^+ states in Ru isotopes near midshell are almost constant, being 242 keV (^{108}Ru), 241 keV (^{110}Ru) and 237 keV (^{112}Ru) but deformation is the largest for ^{108}Ru, i.e. at N=64. The deformation of the midshell nucleus ^{108}Mo is not known very accurately [17] but the 2^+ energies present a clear minimum at N=64 with 172 keV (^{106}Mo), with a slight rise to 192 keV and 193 keV (^{104}Mo and ^{108}Mo), respectively [28,29]. The systematics of levels, Fig. 4, also shows that the excitation energies of the intruder band levels versus neutron number form a V-shape pattern with a sharp edge at the minimum. This behaviour was also noted in a recent study of intruder bands in even-even Cd isotopes [30]. Unfortunately, no comparable data for the immediate Ru and Pd even-even neighbours of Rh are available at these large neutron numbers.

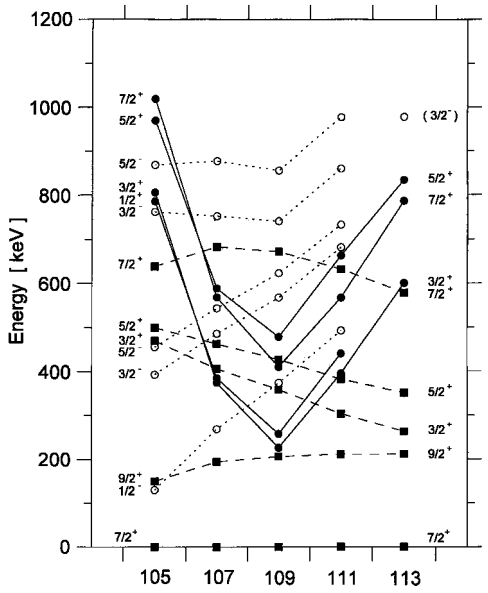

Fig. 4. Level systematics of odd-mass neutron-rich Rh isotopes. Spherical even (resp. odd) parity levels are connected by *dashed* (resp. *dotted*) *lines*. The intruder states are connected by *solid lines*. The extension towards ^{113}Rh is made on the basis of the level scheme in [9,10]

4.3.1 Hindered decays of the deformed $3/2^+$ and $1/2^+$ levels

The $3/2^+$ level at 395 keV in ^{111}Rh was proposed as the lowest-lying member of the deformed band, based on its halflife of 87 ns, which implies a rate of 0.012 single-particle units for the 395 keV E2 transition to the $7/2^+$ ground state [8]. For the similar E2 transition in ^{107}Rh, Kaffrell et al. [2] reported a fairly high rate of 0.16(2) s.p.u., which they were able to explain by mixing of the deformed $3/2^+$ level at 374 keV with the closely lying $3/2^+$ spherical level at 406 keV. Nevertheless, the rates of 0.012 s.p.u. and of 0.018 s.p.u. for the corresponding 226 keV E2 transition in ^{109}Rh [5] compare well. In ^{111}Rh, the $3/2^+$ level can also decay by a 91 keV transition to the spherical $3/2^+$ level at 304 keV. Unfortunately, the conversion coefficient measured in this work is not accurate enough to make definite conclusions about the magnitude of the E2 hindrance in this transition.

The lifetime of the $1/2^+$ 440 keV level has been determined in this work to be 4.8(5) ns. The decay of this deformed $1/2^+$ level proceeds to the spherical $3/2^+$ state by the 137 keV M1 transition which has a rate of 1.8×10^{-3} single-particle units. This value is the first measured rate for the decay of the deformed $1/2^+$ level to a spherical state near the neutron midshell. For the 786 keV $1/2^+$ level in ^{105}Rh, a halflife limit of less than 0.4 ns is given in [10]. The M1 decay to the spherical $3/2^+$ state has a rate larger than 1.1×10^{-3} s.p.u. similar to the rate for the 137 keV transition in ^{111}Rh. However, the E2 decay to the $5/2^+$ single-particle level at 499 keV has a rate larger than 0.04 s.p.u., which could indicate a reduction of the hindrance of E2 transitions with respect to the Rh isotopes near midshell.

4.3.2 Enhanced decays within the K=1/2 band

Indirect evidence for a weak 45 keV transition from the $1/2^+$ to the $3/2^+$ level in ^{111}Rh has been found in this work. The limit of $I_\gamma(45) < 0.5$ relative γ-intensity units converts into $\alpha > 4$, which is consistent with the expected mixture of M1 and E2 multipolarities. In ^{107}Rh and ^{109}Rh, however, this transition has been observed as a γ-ray. In ^{109}Rh, conversion coefficient values of α_k=13(4) [5] and 17(6) [9] were measured for the $1/2^+ \rightarrow 3/2^+$ 32 keV transition and the $1/2^+$ level halflife was determined to be $t_{1/2}$=29 ns [5]. From this, Kaffrell et al. [5] determined a rate of 174(33) s.p.u. and a deformation of β=0.32(3). It would be extremely interesting to obtain more accurate mixing ratios and level lifetimes in order to deduce the quadrupole deformation of the intruder bands with better accuracy. In spite of the limitation of the experimental technique used in this work, estimates for a number of intraband E2 transitions could be obtained, which are listed

Table 4. Rates in Weisskopf units for electric quadrupole transitions in Rh isotopes. Symbols s and d refer to spherical and deformed states, respectively. Values without reference are from this work

Isotope	Level			Transition to			Rate
	[keV]	I^π		[keV]	I^π		[W.u.]
^{107}Rh	374	$3/2^+$	d	374	$7/2^+$	s	0.16(2) [2]
^{109}Rh	226	$3/2^+$	d	226	$7/2^+$	s	0.018 [5]
	258	$1/2^+$	d	32	$3/2^+$	d	174(33) [5]
	359	$3/2^+$	s	358	$7/2^+$	s	> 6
	410	$7/2^+$	d	184	$3/2^+$	d	160(80)
	427	$5/2^+$	s	221	$9/2^+$	s	> 2.8
	478	$5/2^+$	d	221	$1/2^+$	d	> 32
^{111}Rh	304	$3/2^+$	s	304	$7/2^+$	s	> 6
	382	$5/2^+$	s	170	$9/2^+$	s	6(3)
	395	$3/2^+$	d	395	$7/2^+$	s	0.012 [8]
	663	$5/2^+$	d	223	$1/2^+$	d	> 16

in Table 4. In particular, the enhancement of the $7/2^+ \rightarrow 3/2^+$ transition in ^{109}Rh, 160(80), matches very well with the value for the E2 component in the $3/2^+ \rightarrow 1/2^+$ transition [5], as was mentioned above. The limits for the $5/2^+ \rightarrow 1/2^+$ transitions, in both ^{109}Rh and ^{111}Rh, also indicate large enhancements. In conclusion, the intraband E2 transitions may be enhanced by factors of 100–200 for both the $^{109}Rh_{64}$ and $^{111}Rh_{66}$ nuclei.

4.4 Beta feedings

The decay of $I^\pi=5/2^+$ ^{111}Ru to ^{111}Rh populates the $7/2^+$ ground state, with about 50% branching, and levels above 1 MeV. It is remarkable that the β-branches to various $3/2^+$, $5/2^+$ and other $7/2^+$ states below 1 MeV, in spite of their allowed character, are very weak. These features are also observed in the decays of the $I^\pi= 5/2^+$ ground states of ^{107}Ru and ^{109}Ru. The decay of ^{107}Ru to ^{107}Rh proceeds with a 68% branch to the ground state (logft=5.7) [2] and allowed feedings to $(5/2,7/2)^+$ levels at 1042, 1272 and 1306 keV. In the decay of ^{109}Ru, a ground-state branch (logft=7.1) of only 2% is reported [5]. There are no sizeable β-branches up to the $5/2^+$ level at 1027 keV (logft=6.1), and clearly allowed feedings occur only for the levels at 1929 keV (logft=4.9), 1964 keV (logft=5.2) and 2094 keV (logft=5.1). Thus, with the exception of the branching of ^{109}Ru to the ^{109}Rh ground-state, the distribution of the β-feedings in the ^{107}Ru, ^{109}Ru and ^{111}Ru decays shows very similar features.

While the lowest-lying levels in odd-mass Rh isotopes can be interpreted as built on the spherical $g_{9/2}$ and $p_{1/2}$ states, the ground states of their Ru mother nuclei are probably deformed. Neutron-rich even-even Ru isotopes have been extensively studied, via β-decay of Tc [31–33] and prompt-fission experiments [34,35]. The data indicate triaxial deformations with parameters $\beta \simeq 0.3$ [11,20] and γ larger than 20 °. Good descriptions of the levels in ^{108,110}Ru were obtained with the rigid triaxial-rotor model by Shannon et al. [34] and with the rotational-vibrational model by Lu et al. [35], whereas other calculations [36, 37] favour γ-softness even at low spin. The decays of the even-even isotopes ^{110}Ru and ^{112}Ru were recently investigated by Jokinen et al. [21] who observed three strong $0^+ \rightarrow 1^+$ decay branches in both cases. The ground-states of ^{107}Ru, ^{109}Ru and ^{111}Ru have $I^\pi=5/2^+$, as determined in [2,5] and in this work. The decays of odd-Ru nuclei can be understood if the strongly populated states in Rh are formed by coupling the extra odd neutron in Ru to a proton-neutron 1^+ (odd-odd Rh) configuration. This assumption is supported by a comparison of experimental Gamow-Teller strengths in $^{110-112}$Ru decays. B(GT) values of 0.26 and 0.23 were reported in [21] for the decays of ^{110}Ru and ^{112}Ru, respectively. For the ^{111}Ru decay, carrying out the sums on the β-decay branches of allowed character, a B(GT) value of 0.22 is obtained. This value is to be interpreted as a lower limit, since weak β-branches (in terms of intensity) to high-lying levels may have escaped detection. Nevertheless, it compares very well with the values for the even-even neighbouring decays. Theoretical work in the frame of the IBA model [38] accounts fairly well for the $0^+ \rightarrow 1^+$ decays of neutron-rich isotopes in this region. It will be interesting to extend this model to odd nuclei.

In any case, the structure of the odd-mass ruthenium isotopes is not as clear as that of the even-even ones. Prompt-fission data of Butler-Moore et al. [39] show band structure ending on odd-parity levels. Neither in their work nor in a recent β-decay study of ^{111}Tc [40], have assignments been made to the lowest-lying levels in ^{111}Ru. According to the description by Paar [26], the $7/2^+$ Rh ground states have a complex structure with a large $(\pi g_{9/2})^3$ component. Therefore, their β-feeding requires some amplitude of a three-quasiparticle $(\pi g_{9/2})^2_{2^+} \otimes \nu g_{7/2}$ configuration in the ground state of their $5/2^+$ Ru parents. This kind of configuration, but with the $d_{5/2}$ instead of the $g_{7/2}$ neutron, was discussed as being one of the possible components for the $3/2^+$ ground state of ^{105}Ru by Stachel et al. [41].

The hindrances of the β-decays to both the low-lying spherical states and to the deformed intruder band are difficult to understand. A tentative interpretation is to assume that the change of shape between deformed Ru and spherical Rh levels results in large hindrances. Such phenomena are well known in the Sr region [42]. In addition, the hindrances of the Ru decays to the levels in the deformed intruder band could be due to K-hindrance, i.e. ΔK=2 from K=5/2 to K=1/2.

5 Conclusion

In this work, the decay scheme of ^{111}Ru to ^{111}Rh has been extended, now including transitions with absolute branchings $\geq 10^{-3}$. New and intense high-energy transitions have significantly modified the β-feeding pattern, shifting the strength towards the high-energy levels. For some levels in ^{109}Rh and ^{111}Rh, lifetimes have been determined. Branch-

ing ratios and, in some cases, absolute decay rates of γ-rays have been used to determine level spins and parities. The assignment made by Rogowski et al. [8] of an intruder band with its lowest member at 395 keV excitation energy is confirmed, putting the picture of shape coexistence in neutron-rich odd-mass Rh isotopes on a firm ground. The transition rates confirm hindrances of the order of 100 for the decays from the excited intruder bands to the spherical states. They also provide an estimate of the enhancement of E2 transitions within the intruder band of 100 – 200. These features seem to be very similar for ^{109}Rh, where the excited band lies lowest, and ^{111}Rh, at the neutron midshell.

A further determination of the characteristics of both the low-lying spherical states (in particular the ground state of seniority 3) and of the intruder band will require dedicated techniques for the measurements of δ(E2/M1) mixing ratios and of level lifetimes in the subnanosecond range. The present experiments have, however, shown that, within acceptable measurement times, these challenging measurements can be performed at IGISOL. On the other hand, it is also valuable to extend the systematics beyond the neutron midshell. A new β-decay study of ^{113}Ru was performed recently, and is under evaluation [43].

This work was supported by the German DAAD under contract DFG(Kr806/5) and the Academy of Finland. Several of us were supported by the Research Council of Norway (J.A., J.P.O.) and the Swedish Natural Research Council (R.M., G.S.).

References

1. Rogowski J., Kaffrell N., De Frenne D., Heyde K., Jacobs E., Harakeh M.N., Schippers J.M., and van der Werf S.Y.: Phys. Lett. **B207**, 125 (1988)
2. Kaffrell N., Hill P., Rogowski J., Tetzlaff H., Trautmann N., Jacobs E., de Gelder P., De Frenne D., Heyde K., Skarnemark G., Alstad J., Blasi N., Harakeh M.N., Sterrenburg W.A., and Wolfsberg K.: Nucl. Phys. **A460**, 437 (1986)
3. Kaffrell N., Rogowski J., Tetzlaff H., Trautmann N., De Frenne D., Heyde K., Jacobs E., Skarnemark G., Alstad J., Harakeh M.N., Schippers J.M., van der Werf S.Y., Daniels W.R., and Wolfsberg K.: Proc. of 5^{th} Int. Conf. on Nuclei far from Stability, Rosseau Lake, Ontario, Canada 1987 (ed. I. Towner) AIP, New York 1988, p. 286
4. Fogelberg B., Lund E., Zongyuan Y., and Ekström B.: ibid, p. 296
5. Kaffrell N., Hill P., Rogowski J., Tetzlaff H., Trautmann N., Jacobs E., de Gelder P., De Frenne D., Heyde K., Börjesson S., Skarnemark G., Alstad J., Blasi N., Harakeh M.N., Sterrenburg W.A., and Wolfsberg K.: Nucl. Phys. **A470**, 141 (1987)
6. Persson H., Skarnemark G., Skålberg M., Alstad J., Liljenzin J.O., Bauer G., Haberberger F., Kaffrell N., Rogowski J., and Trautmann N.: Radiochim. Acta **48**, 177 (1989)
7. Skarnemark G., Alstad J., Kaffrell N. and Trautmann N.: J. Radioanal. Nucl. Chem. **142**, 145 (1990)
8. Rogowski J., Alstad J., Fowler M.M., De Frenne D., Heyde K., Jacobs E., Kaffrell N., Skarnemark G., and Trautmann N.: Z. Phys. **A337**, 233 (1990)
9. Penttilä H.: PhD Thesis, University of Jyväskylä, (1992)
10. Firestone R.B.: Table of Isotopes, 8^{th} Edition, John Wiley & Sons INC. , New York, 1996
11. Schoedder S., Lhersonneau G., Wöhr A., Skarnemark G., Alstad J., Nähler A., Eberhardt K., Äystö J., Trautmann N., and Kratz K.-L.: Z. Phys. **A352**, 237 (1995)
12. Essel H.G., Grein H., Kroll T., Kynast W., Richter M., Sohlbach H., Spreng W., Winkelmann K., and Müller W.F.J.: IEEE Trans. on Nucl. Sci. **NS-34**, 907 (1987)
13. Klöckl I., Pfeiffer B., Schoedder S., Lhersonneau G., Kratz K.-L., Dendooven P., and the IGISOL-Collaboration: Verhandl. DPG(VI)32, HK32.6 (1997)
14. Penttilä H., Dendooven P., Honkanen A., Huhta M., Jauho P.P., Jokinen A., Lhersonneau G., Oinonen M., Parmonen J.M., Peräjärvi K., and Äystö J.: Proc. EMIS-13, Bad Dürkeim, Germany 1996, Nucl. Instr. Methods **B126**, 213 (1997)
15. Huhta M., Dendooven P., Honkanen A., Lhersonneau G., Oinonen M., Penttilä H., Peräjärvi K., Rubchenya V., and Äystö J.: ibid, p. 201
16. Lhersonneau G., Dendooven P., Honkanen A., Huhta M., Oinonen M., Penttilä H., Äystö J., Kurpeta J., Persson J.R., and Popov A.: Phys. Rev. **C54**, 1592 (1996)
17. Penttilä H., Dendooven P., Honkanen A., Huhta M., Lhersonneau G., Oinonen M., Parmonen J.M., Peräjärvi K., Äystö J, Kurpeta J. and Persson J.R.: Phys. Rev. **C54**, 2760 (1996)
18. Jääskeläinen K., Jones P.M., Lampinen A., Loberg K., and Trzaska W.: JYFL Annual Report 1995, p.15
19. Lhersonneau G.: Nucl. Instr. Methods **157**, 349 (1978)
20. Mach H., Fogelberg B., Sanchez-Vega M., Aas A.J., Erokhina K.I., Gulda K., Isakov V.I., Kvasil J., and Lhersonneau G.: Proc. Int. Workshop on Physics of Unstable Nuclear Beams, Serra Negra, Brazil (1996), World Scientific, Singapore 1997, p. 338.
21. Jokinen A., Äystö J., Dendooven P., Eskola K., Janas Z., Jauho P.P., Leino M., Parmonen J.M., Penttilä H., Rykaczewski K., and Taskinen P.: Z. Phys. **A 340**, 21 (1991)
22. Blachot J.: NDS **64**, 913 (1991)
23. Clark R.G., Glendenin L.E. and Talbert W.L.: Proc. Symp. on Physics and Chemistry of Fission, Rochester, New York, USA, IAEA, Vienna 1974, p. 221.
24. Penttilä H., Taskinen P., Jauho P., Koponen V., Davids C.N., and Äystö J.: Phys. Rev. **C38**, 931 (1988)
25. Blachot J.: NDS **77**, 299 (1996)
26. Paar V.: Nucl. Phys. **A211**, 29 (1973)
27. Wöhr A., Gabelmann H., Lhersonneau G., Pfeiffer B., Kratz K.-L. and the ISOLDE-Collaboration: Proc. 6^{th} Int. Conf. on Nuclei far from Stability, Bernkastel-Kues, Germany 1992 Inst. Phys. Ser. **132**, 867 (1993)
28. Hotchkis M.C.A., Durell J.L., Fitzgerald J.B., Mowbray A.S., Philips W.R., Ahmad I., Carpenter M.P., Janssens R.V.F., Khoo T.L., Moore E.F., Benet Ph., and Ye D.: Nucl. Phys. **A530**, 111 (1991)
29. Guessous A., Schulz N., Bentaleb M., Lubkiewicz E., Durell J.L., Pearson C.J., Philips W.R., Shannon J.A., Urban W., Varley B.J., Ahmad I., Lister K., Morss L.R., Nash K.L., Williams C.W., and Khazrouni S.: Phys. Rev. **C53**, 1191 (1996)

30. Juutinen S., Julin R., Jones P., Lampinen A., Lhersonneau G., Mäkela E., Piiparinen M., Savelius A., and Törmänen S.: Phys. Lett. **B 386**, 80 (1996)
31. Äystö J., Jauho P.P., Janas Z., Jokinen A., Parmonen J.M., Penttilä H., Taskinen P., Béraud R., Duffait R., Emsallem A., Meyer J., Meyer M., Redon N., Leino M., Eskola K., and Dendooven P.: Nucl. Phys. **A515**, 365 (1990)
32. Stachel J., Kaffrell N., Trautmann N., Brodén K., Skarnemark G., and Eriksen D.: Z. Phys. **A316**, 105 (1984)
33. Sümmerer K., Kaffrell N., Stender E., Trautmann N., Brodén K., Skarnemark G., Björnstad T., Haldorsen I., and Maruhn J.A.: Nucl. Phys. **A339**, 74 (1980)
34. Shannon J.A., Philips W.R., Durell J.L., Varley B.J., Urban W., Pearson C.J., Ahmad I., Lister C.J., Moss L.R., Nash K.L., Williams C.W., Schulz N., Lubkiewicz E., and Bentaleb M.: Phys. Lett. **B336**, 136 (1994)
35. Lu Q.H., Butler-Moore K., Zhu S.J., Hamilton J.H., Ramayya A.V., Oberacker V.E., Ma W.C., Babu B.R.S., Deng J.K., Kormicki J., Cole J.D., Aryaeinejad R., Dardenne Y.X., Drigert M., Peker L.K., Rasmusen J.O., Stoyer M.A., Chu S.Y., Gregorich K.E., Lee I.Y., Mohar M.F., Nitschke J.M., Johnson N.R., McGowan F.K., Ter-Akopian G.M., Oganessian Yu.Ts., and Gupta J.B.: Phys. Rev. **C52**, 1348 (1995)
36. Troltenier D., Draayer J.P., Babu B.R.S., Hamilton J.H., Ramayya A.V., and Oberacker V.E.: Nucl. Phys. **A 601**, 56 (1996)
37. Skalski J., Mizutori S. and Nazarewicz W.: Nucl. Phys. A **617**, 282 (1997)
38. Maino G. and Zuffi L.: Proc. 5^{th} International Seminar on Nuclear Physics, Ravello, World Scientific, Singapore (1995), p. 611
39. Butler-Moore K., Aryaeinejad R., Cole J.D., Dardenne Y., Greenwood R.G., Hamilton J.A., Ramayya A.V., Ma W.-C., Babu B.R.S., Rasmussen J.O., Stoyer M.A., Chu S.Y., Gregorich K.E., Mohar M., Asztalus S., Prussin S.G., Moody K.J., Lougheed R.W., and Wild J.F.: Phys. Rev. **C52**, 1339 (1995)
40. Pfeiffer B. et al.: to be submitted to Z. Phys. **A**
41. Stachel J., Kaffrell N., Stender E., Sümmerer K., Trautmann N., Brodén K., Skarnemark G., Björnstad T., and Haldorsen I.: Radiochimica Acta **26**, 127 (1979)
42. Lhersonneau G., Pfeiffer B., Kratz K.-L., Ohm H., Sistemich K., Brant S., and Paar V.: Z. Phys. **A 337**, 149 (1990)
43. Kurpeta J., Penttilä H., Dendooven P., Honkanen A., Huhta M., Lhersonneau G., Oinonen M., Peräjärvi K., Plochocki A., Wang J.C. and Äystö J.: JYFL Annual Report 1996, p. 29 (1997)